X-ray Structure of the Magnesium(II)-Pyrophosphate Complex of the Truncated Head of Dictyostelium discoideum Myosin to 2.7 .ANG. Resolution

ARTICLE *in* BIOCHEMISTRY · AUGUST 1995

Impact Factor: 3.02 · DOI: 10.1021/bi00028a005 · Source: PubMed

2 AUTHORS:

Clyde A Smith
Stanford University
92 PUBLICATIONS **3,213** CITATIONS
SEE PROFILE

Ivan Rayment
University of Wisconsin–Madison
232 PUBLICATIONS **14,628** CITATIONS
SEE PROFILE

X-ray Structure of the Magnesium(II)−Pyrophosphate Complex of the Truncated Head of *Dictyostelium discoideum* Myosin to 2.7 Å Resolution[†,‡]

Clyde A. Smith and Ivan Rayment*

Institute for Enzyme Research and Department of Biochemistry, University of Wisconsin, Madison, Wisconsin 53705

Received April 10, 1995; Revised Manuscript Received May 9, 1995[⊗]

ABSTRACT: The structure of the magnesium pyrophosphate complex of the truncated head of *Dictyostelium* myosin has been determined by molecular replacement at 2.7 Å resolution and refined to a crystallographic *R*-factor of 16.0%. The crystals belong to the orthorhombic space group $P2_12_12$, where $a = 105.2$ Å, $b = 182.1$ Å, and $c = 54.5$ Å. The conformation of the protein around the magnesium pyrophosphate is very similar to that seen when magnesium ADP−beryllium fluoride binds in the active site. The latter complex mimics the binding of ATP prior to hydrolysis. The pyrophosphate molecule occupies the β- and γ-phosphate sites, where the two phosphorus atoms are in the same positions as the β-phosphate and the BeF_x moiety of the beryllium fluoride-trapped ADP. The surrounding active site residues are almost perfectly superimposable in the two structures and the hydrogen-bonding interactions that the PP_i makes with the protein are essentially identical. The similarity between the MgPPi and MgADP•BeFx complex with S1Dc suggests that the conformational change, which occurs when ATP binds to actomyosin and which reduces the affinity of myosin for actin, is caused by the binding of the γ- and β-phosphate groups of the nucleotide. This then implies that the role of the remainder of the substrate is to increase the binding affinity for myosin and thus to drive the equilibrium toward dissociation of myosin from actin.

Myosin is an enzyme that, in conjunction with actin, transduces the chemical energy from the hydrolysis of ATP into directed mechanical movement. The actomyosin system of motility is found in all eukaryotic cells where it is directly involved in cytokinesis, cell division, and movement of organelles. In its most abundant and organized state it is responsible for muscle contraction. Over the years considerable effort has been devoted toward understanding the molecular origin of the myosin-based motility. Extensive kinetic measurements on both fragments of myosin and muscle fibers have established the chemical and physical features of this process. The classic work of Lymn and Taylor provided the first successful description of the contractile cycle (Lymn & Taylor, 1971). This demonstrated that ATP hydrolysis by myosin occurred during the time that myosin was dissociated from actin and suggested that the power stroke was associated with product release. This has been verified by measurements on muscle fibers that show that the power stroke is triggered by the loss of inorganic phosphate (Goldman, 1987). Subsequent kinetic studies have established that the contractile cycle is considerably more complex than originally described by Lymn and Taylor and requires the introduction of weak and strong binding states into the description of the actomyosin complex (Eisenberg & Greene, 1980; Geeves et al., 1984; Stein et al., 1979). In addition, kinetic analysis reveals that nucleotide binding and release is a multistep process suggesting that ATP hydrolysis involves the transition between several discreet conformational states (Bagshaw & Trentham, 1974; Trybus & Taylor, 1982).

Interpretation of the chemical and structural steps underlying the contractile cycle has been aided considerably by the use of nucleotide analogs that mimic ATP and its hydrolysis products (Greene & Eisenberg, 1980; Trybus & Taylor, 1982; Yount et al., 1971). As a group, these compounds have provided opportunities to trap myosin at distinct points around the contractile cycle. Derivatives such as AMPPNP, ATPγS, and pyrophosphate have been useful for investigating the properties of the weak-binding states of myosin for actin. Pyrophosphate is of particular interest, since it represents the smallest molecule that will substantially reduce the affinity of myosin for actin (Greene & Eisenberg, 1980). There is an extensive literature describing the effects of nucleotide analogs on the chemical and physiological properties of actin and myosin. Even so, it has been difficult to correlate the effects of nucleotide analogs on the physiological and chemical behavior of actomyosin due to a lack of information concerning the effect of nucleotides on structure of the myosin head.

The X-ray structure determinations of both actin and myosin partially solved the problem of connecting the biochemical and physiological studies by providing a structural hypothesis for the contractile cycle (Holmes et al., 1990; Kabsch et al., 1990; Rayment et al., 1993a,b). However, the initial structure determination of the myosin head was carried out in the absence of ATP or a substrate analog. Furthermore, the model building studies, based on a combination of electron microscopy and X-ray structures of actin and myosin, strongly suggested that myosin undergoes conformational changes when it binds to actin and to ATP (Rayment et al., 1993a). In an effort to investigate the nature

[†] This research was supported in part by NIH Grant AR35186 to I.R. C.A.S. is supported by Grant TW05194 from the Fogarty International Centre of the National Institutes of Health.

[‡] The X-ray coordinates have been deposited in the Brookhaven Protein Data Bank (file name 1MNE).

* To whom correspondence should be addressed at the Institute for Enzyme Research, University of Wisconsin, 1710 University Ave., Madison, WI 53705 [telephone (608) 262-0529; Fax (608) 265-2904].

[⊗] Abstract published in *Advance ACS Abstracts,* July 1, 1995.

0006-2960/95/0434-8973$09.00/0

of the structural transitions that occur during the process of energy transduction, the three-dimensional structures of a series of ATP analogs with a truncated head of myosin from *D. discoideum* have been undertaken. The structures of the truncated head of *Dictyostelium discoideum* myosin II (S1Dc)[1] with ADP trapped in the active site with beryllium and aluminum fluoride have been reported (Fisher et al., 1995). These complexes are analogs of ATP and the hydrolysis transition state, respectively, and represent distinct points in the middle of the contractile cycle. To fully understand the structural transitions that underlie the contractile cycle and to correlate the biochemical and physiological studies on muscle contraction, it is necessary to know the conformation of myosin at earlier stages of nucleotide binding such as that induced by magnesium pyrophosphate. Here we report the crystallographic analysis of the Mg^{2+}−pyrophosphate complex of the *Dictyostelium* myosin motor to 2.7 Å resolution.

EXPERIMENTAL PROCEDURES

Protein Purification and Crystallization. Myosin subfragment-1 from *D. discoideum* (S1Dc) was truncated genetically just prior to the light chain binding region, as judged by inspection of the chicken skeletal myosin S1 structure (Rayment et al., 1993b) and sequence alignment, producing a fragment of 761 amino acids extending from Asp 2 to Asn 762. The truncated myosin head was purified in a way similar to that described before (Itakura et al., 1993). The *D. discoideum* cells containing the engineered myosin head were grown in HL5 medium at 22 °C by continuous agitation in 5 L conical flasks. At saturation ($\approx 1-2 \times 10^7$ cells/cm^3), the cells were harvested by centrifugation, washed with 10 mM Tris-HCl, pH 8, and frozen in liquid N_2. The cells (≈50−60 g) were ruptured by sonication in 20 mM Bis-Tris-propane (BTP), pH 7.5, containing 25 mM NaCl, 4 mM EDTA, 1 mM DTT, and 0.2 mM phenylmethanesulfonic acid (PMSF), and the cellular debris was removed by low-speed centrifugation (1000*g*). The cytoskeletal components, including the truncated myosin head, were collected by high-speed centrifugation at 235000*g* rpm, and the myosin was extracted by homogenizing the pellets in 20 mM BTP, 50 mM NaCl, 7 mM $MgCl_2$, 6 mM ATP, 1 mM DDT, and 0.2 mM PMSF. Following removal of the actin and other cytoskeletal components by further high-speed centrifugation at 235000*g*, the crude myosin was applied to a 50 mL Toyopearl DEAE-650M column. The S1Dc was collected in the flowthrough, residual actin remaining bound to the column.

The S1Dc was made 35% saturated with ammonium sulfate, stirred for 1 h at 4 °C, and centrifuged at 44000*g*. Additional ammonium sulfate was added to bring the supernatant to 70% saturation, and it was left to stand at 4 °C overnight. The precipitated myosin was collected by centrifugation (44000*g*), dialyzed against 50 mM Tris-HCl, pH 8.0, 100 mM KCl, 2 mM $MgCl_2$, 1 mM DTT, 0.2 mM NaN_3, and 0.2 mM PMSF, and applied to an ATP affinity column. S1Dc was eluted with 50 mM Tris-HCl, pH 8.0, containing 2 mM NaP_2O_7 (sodium pyrophosphate), 100 mM KCl, 2 mM EDTA, 1 mM DTT, and 0.2 mM NaN_3. Finally, the purified S1Dc was concentrated to about 8−10 mg/mL and the buffer exchanged to 10 mM Hepes, pH 8.0, 100 mM NaCl, 2 mM $MgCl_2$, 0.2 mM NaN_3, and 1 mM DTT in an Amicon microcentricon (10 kDa exclusion limit).

Crystals of the magnesium pyrophosphate complex ($MgPP_i$·S1Dc) were grown by microbatch from 8.5% PEG 8000, 25 mM Hepes, pH 7.0, 100 mM NaCl, and 2 mM DTT. The protein concentration in the final drop was 5 mg/mL. Crystallization was initiated by the introduction of microseeds from preliminary hanging-drop experiments. Initial batch trials produced thin, almost two-dimensional plates. In order to thicken the plates, a number of organic additives at varying concentrations were tried, including 2-methyl-2,4-pentanediol, 1,5-pentanediol, and octyl β-glucoside. It was found that 2.7% ethylene glycol (EG) produced crystals suitable for X-ray diffraction studies. The original design of this crystallization experiment was to grow crystals of the apoenzyme. However, in retrospect, the protocol for buffer exchange and protein concentration did not remove sufficient magnesium pyrophosphate to attain this state. It is estimated from the number and magnitude of each buffer exchange that the residual concentration of $MgPP_i$ was between 0.2 and 2 μM. Given that the association constant for rabbit skeletal muscle myosin subfragment-1 and $MgPP_i$ at 4 °C is 2.3×10^6 M^{-1} (Greene & Eisenberg, 1980) and that *Dictyostellium* myosin has a similar catalytic mechanism though somewhat different association constants for ATP (Ritchie et al., 1993), it is expected that most of the enzyme will be bound to magnesium pyrophosphate. The electron density is consistent with an occupancy of close to unity.

Data Collection and Processing. The $MgPP_i$·S1Dc crystals belong to space group $P2_12_12$ with unit cell dimensions a = 105.2 Å, b = 182.1 Å, and c = 54.5 Å and are isomorphous with crystals of the beryllium fluoride-trapped ADP complex of S1Dc, MgADP·BeF_x·S1Dc (cell dimensions a = 105.3 Å, b = 182.6 Å, and c = 54.7 Å) (Fisher et al., 1995). They contain one molecule per asymmetric unit; the calculated packing volume, V_M, based upon a molecular mass of 87 000, is 3.0 Å^3/Da, indicating a solvent content of approximately 59% (Matthews, 1968). X-ray data were collected from four crystals on an Siemens Hi-STAR area detector, mounted on a Rigaku RU200 operating at 50 kV and 50 mA, with Supper double-focusing mirrors. The temperature of the crystals was maintained at 4 °C by a stream of cooled dry air. The images were processed with the program XDS (Kabsch, 1988a,b), and the data from each crystal were internally scaled in shells using the program XSCALIBRE (G. Wesenberg and I. Rayment, unpublished results). Although there were some reflections observed out to 2.6 Å, only data to 2.65 Å were included during final merging and scaling, to give a data set of 25 880 independent reflections with an R_{merge} of 5.1%. One crystal showed poor correlation with the others and was discarded in this final intercrystal scaling step. This crystal was smaller and diffracted to lower resolution than the others. There is a marked decrease in the number of unique reflections and those with $I > 2\sigma_F$ beyond 3.1 Å, as indicated in Figure 1,

[1] Abbreviations: myosin S1, myosin subfragment-1; S1Dc, *Dictyostelium discoideum* myosin motor domain; PMSF, phenylmethanesulfonic acid; BTP, Bis-Tris-propane; $MgPP_i$·S1Dc, magnesium pyrophosphate complex of truncated *D. discoideum* myosin head; EG, ethylene glycol; MgADP·BeF_x·S1Dc, the beryllium fluoride−ADP complex of *D. discoideum* myosin head; MgADP·AlF_4·S1Dc, the aluminum fluoride−ADP complex of *D. discoideum* myosin head; PP_i, pyrophosphate, P_2O_7; P-loop, phosphate binding loop found in nucleotide-dependent enzymes.

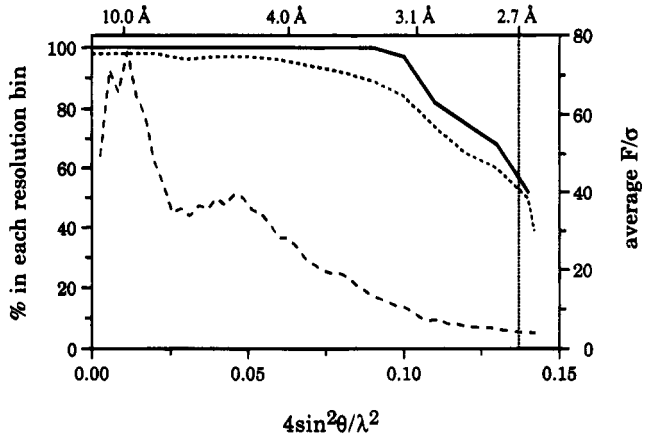

FIGURE 1: Percentage of the theoretical number of reflections (—) and those unique reflections with $F > 2\sigma_F$ (- - -), as a function of 4 $\sin^2 \theta/\lambda^2$ for the final $MgPP_i$·S1Dc data set. The percentages were calculated in bins of $\Delta 4 \sin^2 \theta/\lambda^2 = 0.01$ Å^{-2}. Also shown is a plot of the average F/σ (— —) as a function of 4 $\sin^2 \theta/\lambda^2$. The averages were calculated in bins of $\Delta 4 \sin^2 \theta/\lambda^2 = 0.003$ Å^{-2}.

Table 1: X-ray Data Processing

no. of crystals used	3
max resolution (d_{min}, Å)	2.7
total reflections measured to d_{min}	50000
independent reflections to d_{min}	25455
R_{merge} (%)[a]	5.1
theoretical no. of reflections to d_{min}	27773
cumulative % completeness	92
% completeness in highest resolution shell[b]	58
unit cell parameters	
a (Å)	105.2
b (Å)	182.1
c (Å)	54.5

[a] $R = \sum|I - \bar{I}|/\sum I \times 100$. [b] 2.70–2.80 Å.

although at the resolution limit of 2.7 Å used for refinement, there is still a significant proportion of the unique reflections (>50%) having $F > 2\sigma_F$. The variation of the average F/σ is also indicated in Figure 1, and it should be noted that, at the nominal resolution cutoff of 2.7 Å, the average $F/\sigma \approx 4.1$. Relevant data collection and processing statistics are given in Table 1.

Structure Determination and Refinement. Given the isomorphism of the $MgPP_i$·S1Dc crystals with those of MgADP·BeF_x·S1Dc, the starting model for refinement was derived from the refined 2.0 Å model for MgADP·BeF_x·S1Dc (Fisher et al., 1995), with the Mg^{2+} ion, the MgADP·BeF_x·S1Dc moiety, and the solvent molecules removed. The individual temperature factors (B-values) for all protein atoms were set to a uniform value of 30.0 Å^2; the overall B-value based upon a Wilson plot (Wilson, 1942) was estimated to be ≈29.5 Å^2. The initial R-factor for all data between 10.0 and 2.8 Å was 32.2%. The structure was refined by conventional restrained least squares with the program TNT (Tronrud et al., 1987); the first phase of positional refinement (B-values held constant at 30.0 Å^2) lowered the R-factor to 24.0%. Electron density maps calculated at this stage ($2F_o - F_c$ and $F_o - F_c$) were displayed on an Evans and Sutherland PS390 interactive graphics system with the program FRODO (Jones, 1985), clearly indicating extra density in the vicinity of the ATP binding site (as identified in the MgADP·BeF_x·S1Dc structure). A Mg^{2+} ion and a pyrophosphate ion (PP_i) were built into the available density. The positional coordinates and individual temperature factors of the model were then refined using all data between 15.0 and 2.7 Å. The R-factor during this second phase of refinement dropped to 19.8%.

Table 2: Refinement Statistics[a]

resolution limits (Å)	15.0–2.7
initial R-factor[b]	32.2
final R-factor	16.0
no. of reflections used	25307
no. of protein atoms	5887
no. of solvent molecules	148
other molecules, ions	1 Mg^{2+}, 1 $P_2O_7^{2-}$
av B-value, protein atoms (Å^2)	34.4
av B-value, all atoms (Å^2)	34.9
weighted rms deviations from ideality	
bond length (Å)	0.010
bond angles (deg)	2.231
planarity (trigonal) (Å)	0.010
planarity (others) (Å)	0.023
torsional angle (deg)[c]	18.66

[a] TNT refinement. [b] $R = \sum||F_o| - k|F_c||/\sum|F_o| \times 100$. [c] No restraints were placed on torsional angles during refinement.

Special attention was paid to the Mg^{2+} ion and the PP_i during refinement, as at the current resolution, the electron density associated with the $MgPP_i$ could not be readily resolved from the protein density. Bond lengths between the Mg^{2+} and the two protein ligands (Thr 186 and Ser 237) and the two coordinating oxygen atoms on the PP_i were constrained to between 1.9 and 2.1 Å. At two stages in the refinement, the $MgPP_i$ moiety was left out of the coordinate file, and omit $2F_o - F_c$ and $F_o - F_c$ maps were calculated. The $MgPP_i$ was subsequently built back into the available density.

The locations of solvent molecules were found by searching an $F_o - F_c$ electron density map and obtaining a list of peaks above a threshold level of 2.5σ. Water molecules were then placed at each peak position and tested to see whether they fell within a specified distance of a potential hydrogen bond donor or acceptor (typically ≤3.5 Å). The programs PEAKMAX, WATPEAKS, and DISTANG in the CCP4 program suite (CCP4, 1994) were used for these searches. The location of these water molecules was checked manually and discarded unless they made hydrogen bonds of reasonable geometry to neighboring groups and were not close to any parts of the structure whose conformation was in doubt. A total of 148 water molecules were added to the structure in this way. Due to the medium resolution of the data, a complete model for the solvent structure in the molecule could not be determined, but it was deemed necessary to attempt to model the water molecules in and around the active site in order to present the most accurate phasing information possible in this region. Inclusion of these water molecules significantly improved the quality of the electron density for the protein.

RESULTS

The Refined Model. The final model for the $MgPP_i$·S1Dc complex consists of 5887 protein atoms (743 residues), 148 solvent molecules, one Mg^{2+} ion, and a pyrophosphate ion. The crystallographic R-factor for 25 307 reflections between 15.0 and 2.7 Å is 16.0%. The geometry of the final model is very good, the overall rms deviations in bond lengths and bond angles being 0.010 Å and 2.23°, respectively. Relevant refinement statistics are given in Table 2.

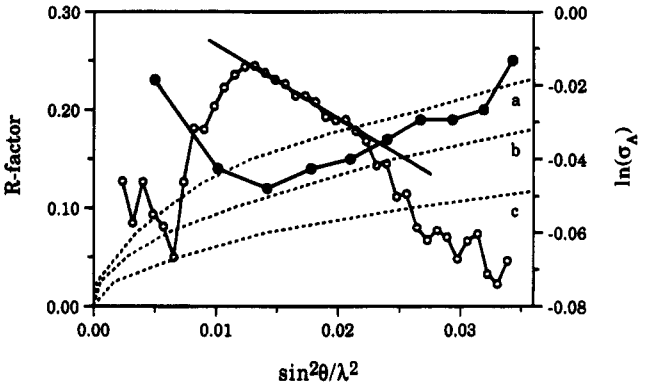

FIGURE 2: Plots of the *R*-factor (●, left axis) and $\ln(\sigma_A)$ (○, right axis) as a function of resolution (expressed as $\sin^2 \theta/\lambda^2$). The theoretical variations of the *R*-factor for coordinate errors, Δr, of 0.15, 0.175, and 0.2 Å are indicated by the dashed curves a, b, and c, respectively.

The average error in the model is estimated from a Luzzati plot (Luzzati, 1952), shown in Figure 2, to be between 0.15 and 0.2 Å. A σ_A plot (Read, 1986), also given in Figure 2, suggests an rms error in the atomic coordinates of 0.24 Å, based upon the slope of the $\ln(\sigma_A)$ versus $\sin^2 \theta/\lambda^2$ plot between 4.5 and 3.5 Å. The deviations from linearity at low resolution (<4.5 Å) arise primarily from the omission of the disordered solvent [the premise that $\ln(\sigma_A)$ is a linear function of $\sin^2 \theta/\lambda^2$ is only valid if the atoms which are missing from the structure have the same overall temperature factor as the atoms included in the structure; clearly, this will not be the case with disordered solvent molecules], while the nonlinearity at high resolution (>3.5 Å) can be attributed to measurement errors and the weakness of the data (Read, 1986).

The values obtained by the two methods agree closely and most probably represent the coordinate error in the majority of the structure. However, the actual error in well-defined regions (the area around the active site and the secondary structure elements, for example) is probably somewhat less than this but substantially more in the poorly defined parts of the molecule, such as the loops forming the junctions between the three tryptic fragments. The electron density in these regions is poor, and although every effort was made to determine their correct conformation with the use of omit maps, they remain ill-defined in relation to the rest of the structure. The only breaks in the polypeptide chain are in these regions (Ala 204−Gly 209 between the 25 and 50 kDa fragments and Ala 621−Ala 627 between the 50 and 20 kDa fragments) and one other part of the molecule (Ala 500−Ala 508), a loop connecting two long helices which form the foundations of the lower domain of the central 50 kDa tryptic fragment.

Correlation coefficients calculated between the observed and calculated structure factors (phased by the final model) also indicate these areas of weak electron density (Figure 3), along with several others. The loops connecting the secondary structure elements in the NH_2-terminal domain, for example, have correlation coefficients lower than the average (0.985), namely, residues near Glu 43, Val 53, Asp 66, and Lys 74−Asp 76. In addition, three small regions in the upper central domain (residues Ala 361−Ala 365, Gly 401−Arg 402, and Glu 444−Ile 455) have values significantly lower than the rest of the structure, and as indicated in Figure 3, parts of the COOH-terminal domain show a lower correlation (Pro 710−Ala 716). A plot of the average main-chain temperature factors (*B*-values) against residue number (also shown in Figure 3) closely corresponds with the correlation coefficient plot (i.e., residues with high average *B*-values again indicating the poorer regions of the structure).

A Ramachandran plot (Ramakrishnan & Ramachandran, 1965) of the main-chain conformational angles (Figure 4) indicates that virtually all the non-glycine and non-proline residues lie within or very close to the allowed regions of conformational space. A representative section of the $2F_o - F_c$ electron density map is shown in Figure 5.

Polypeptide Chain Folding and Domain Structure. The overall molecular structure of the motor domain of *dictyostelium* myosin II has been described previously (Fisher et al., 1995) and is essentially similar to the observed chicken skeletal myosin S1 structure (Rayment et al., 1993b). The topology of the $MgPP_i$·S1Dc molecule as observed here is identical to the MgADP·BeF_x·S1Dc structure. Historically, the S1 structure has been described in terms of the three major tryptic fragments (Balint et al., 1975; Mornet et al.,

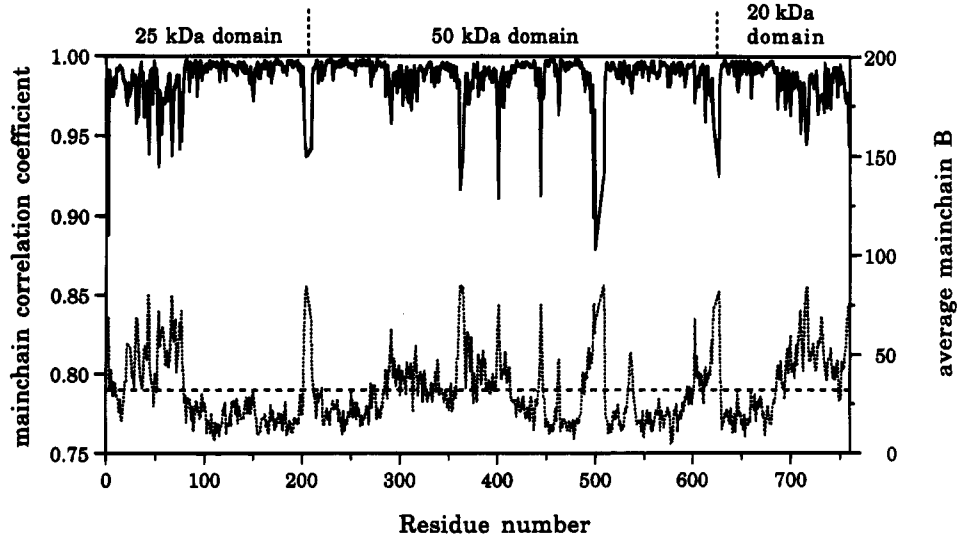

FIGURE 3: Plot of the variation of the average main-chain temperature factor (dashed lines) and the main-chain correlation coefficient (solid lines) with residue number. The correlation coefficients were calculated with the program OVERLAPMAP (CCP4, 1994).

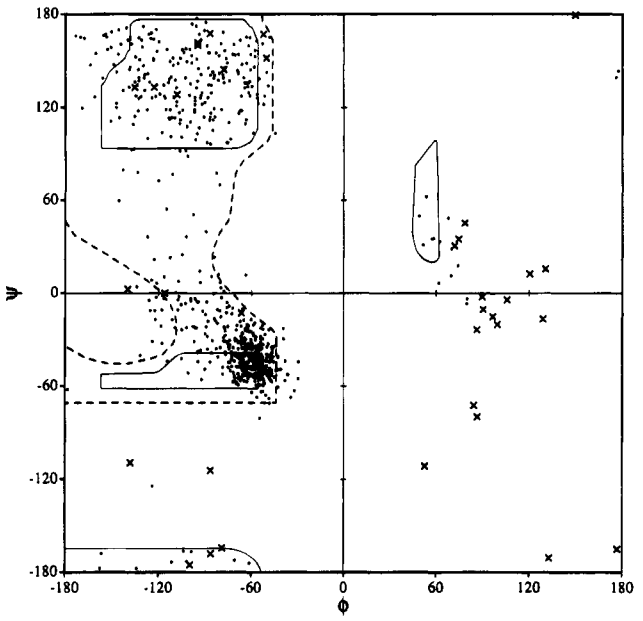

FIGURE 4: Plot of the main-chain conformational torsion angles ϕ and ψ for the final $MgPP_i$·S1Dc model. All non-glycinal dihedral angles are indicated as dots whereas the glycinal angles are shown as crosses (44 in total). Fully allowed ϕ and ψ values are enclosed by continuous lines; those only partially allowed are enclosed by broken lines.

1979): the NH_2-terminal or 25 KDa fragment formed by residues Asp 2−Ala 204 (S1Dc residue numbering), the central, 50 kDa fragment (Gly 209−Ala 621), and the COOH-terminal, 20 kDa fragment (Ala 627−Ala 759). Although the tryptic fragments themselves do not form independent folding motifs, the myosin head can be viewed in terms of several discrete domains. These have now been shown to be capable of movement relative to each other (Fisher et al., 1995). Since each of these domains is formed primarily from one of the tryptic fragments, it is convenient to retain the earlier nomenclature when discussing the structure.

Active Site. Only protein atoms were included in the starting model (anions, cations, and solvent molecules were removed) in order to provide an unbiased view of the active site. Electron density for the Mg^{2+} ion was clearly observed in both the initial $2F_o - F_c$ and the $F_o - F_c$ maps. Contouring the $2F_o - F_c$ map at 6σ allowed a Mg^{2+} ion to be built unambiguously into an electron density peak between the side chains of Thr 186 and Ser 237. Inclusion of this metal ion left a large piece of bilobal electron density adjacent to the Mg^{2+} position. Examination of the purification procedure suggested that a pyrophosphate (PP_i) ion was the most likely candidate for this extra density. The location of a pyrophosphate ion was determined from the position of the two phosphorus atoms that could be readily seen when the map was contoured at a level of 8σ. Figure 6 shows the final $2F_o - F_c$ electron density map with the final MgPPi model superimposed, while a schematic representation of the active site residues and the $MgPP_i$ is given in Figure 7, showing the interactions between the protein and the $MgPP_i$ molecule.

The nucleotide binding pocket lies at the bottom of a cleft between the 25 kDa and the 50 kDa domains and is flanked by a seven-stranded mostly parallel β-sheet (Figure 8) where the first and sixth strand run in the opposite direction to other five. Three strands (Tyr 116−Ser 119, Phe 122−Val 126, and Gln 173−Gly 179) belong to the 25 kDa fragment, three from the 50 kDa fragment (Gly 240−Phe 247, Ile 253−Tyr 261, and Tyr 448−Ser 456), and the seventh from the 20 kDa fragment (Asn 649−Ile 656). The strand between Tyr 448 and Ser 456 contains the consensus sequence D-X-X-G at its C-terminus, which has been shown to be conserved in the G-proteins and *ras* (Bourne et al., 1991) and is the region which undergoes a conformational change when AlF_4^- is substituted for BeF_3 as the ADP-trapping agent (Fisher et

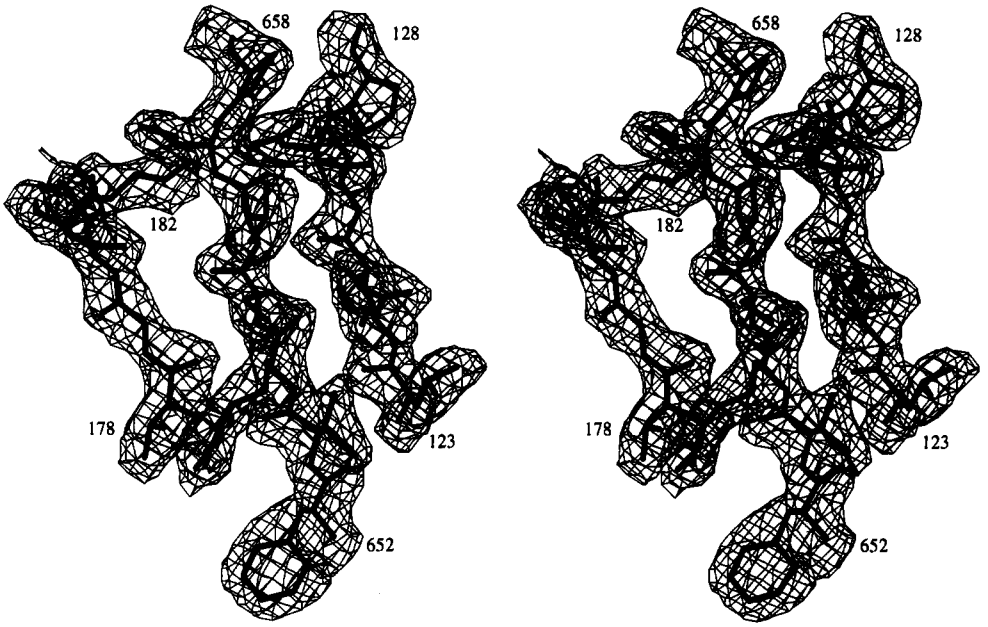

FIGURE 5: Stereoview of a piece of representative $2F_o - F_c$ electron density. Part of the central seven-stranded β-sheet is shown: from the left, Thr 178−Gly 182, Phe 652−Pro 658, and Leu 123−Pro 128. The active site (not shown) lies to the upper left. The first strand, Thr 178−Gly 182, leads into the phosphate binding loop, while the loop directly following Pro 128 at the top to the third strand contains residues that interact with the adenine of ADP in the structure of MgADP·BeF_x·S1Dc. This adenine binding pocket is filled with water molecules in the structure of MgPPi·S1Dc presented here.

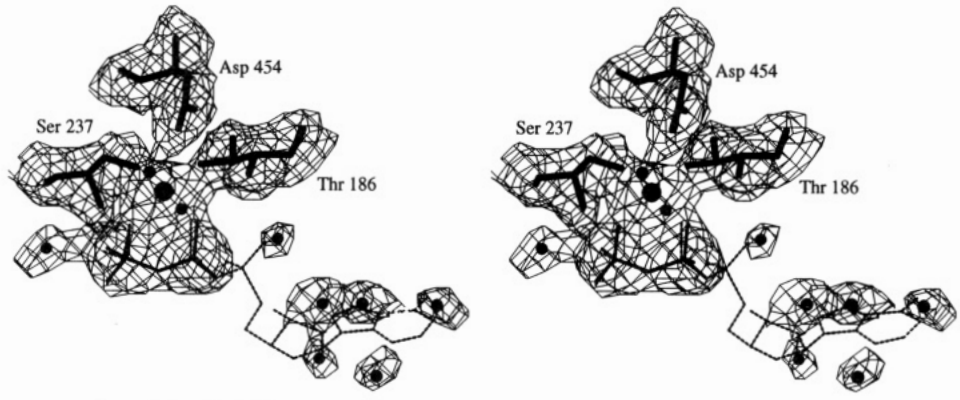

FIGURE 6: Stereo representation of the final $2F_o - F_c$ map showing the magnesium (large solid circle), the two protein ligands, Thr 186 and Ser 237, and the pyrophosphate (solid lines), along with the MgADP•BeF_x moiety from the MgADP•BeF_x•S1Dc structure superimposed (dashed lines). Several water molecules are shown, one adjacent to the pyrophosphate and others occupying the adenine binding site. In order to clearly show the density associated with the $MgPP_i$, the water molecules, and the protein ligands, density more than 1.0 Å from the chosen atoms was set to zero.

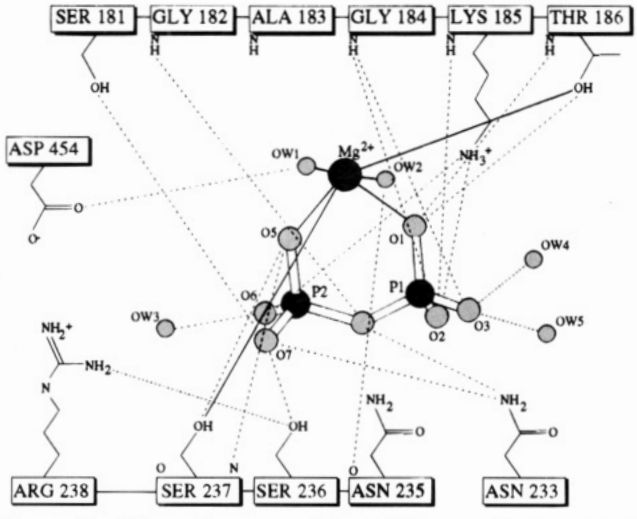

FIGURE 7: Schematic representation of the coordination of the $MgPP_i$ in the phosphate binding pocket.

al., 1995). Also, as in the G-proteins, Asp 454 of the consensus sequence is bound to a water molecule that is part of the coordination sphere of the magnesium ion. The phosphate binding loop (P-loop, residues Gly 179−Thr 186) follows the central strand of this sheet and then runs into a helix (Thr 186−Ala 199) which extends back antiparallel to the strand, lining the active site cleft. The sequence of the P-loop (GESGAGKT) is completely conserved in all myosins and is analogous in terms both of sequence and structure to the P-loops in a number of nucleotide binding proteins including P21 H-*ras* (Pai et al., 1990), adenylate kinase (Diederichs & Schulz, 1990; Muller & Schulz, 1992), recA (Story & Steitz, 1992), transducin α (Noel et al., 1993; Sondek et al., 1994), elongation factor Tu (Kjeldgaard et al., 1993), G_{ial} (Coleman et al., 1994), and F_1-ATPase (Abrahams et al., 1994).

The residues of the P-loop supply a significant number of hydrogen-bonding interactions to the PP_i molecule, namely, the amide nitrogen atoms of Gly 182, Gly 184, Lys 185, Thr 186, and Glu 187 (Figure 9). In addition, the side chain of Lys 185 wraps around the PP_i and hydrogen bonds to one of the phosphate oxygen atoms. One of the phosphate groups (P1) of the PP_i occupies the β-phosphate position as observed in both MgADP•BeF_x•S1Dc and AlF_4•MgADP•S1Dc, while the other phosphate group (P2) occupies the putative γ-phosphate site, as identified by the location of the BeF_x ion in MgADP•BeF_x•S1Dc (Fisher et al., 1995). Two of the oxygen atoms of this P1 phosphate group (O1 and O2) interact via hydrogen bonds to the amide nitrogens of three P-loop residues (Gly 184, Lys 185, and Thr 186) and the side chains of Lys 185 and Thr 186, while the third, which would correspond to the bridging oxygen between the α- and β-phosphates of ADP, interacts only with two solvent molecules. The bridging oxygen between P1 and P2 forms a hydrogen bond to the amide nitrogen of Gly 182 and with the side chain $N_{\delta 2}$ atom of Asn 233. Interestingly, the oxygen atoms of the P2 phosphate do not interact with the main-chain atoms of the P-loop residues, although they do form hydrogen bonds with the side chains of Ser 181 and Lys 185 and with the side chains of Asn 233 and the amide hygrogen of Ser 237. In addition, there is a solvent molecule located adjacent to the P2 phosphate, close to the location of the water molecule observed in the MgADP•BeF_x complex that has been implicated in the catalytic mechanism (Fisher et al., 1995). This water molecule is hydrogen bonded to one of the P2 oxygen atoms but does not make the same hydrogen-bonded contacts to the rest of the protein as does the water in MgADP•BeF_x.

The PP_i contributes two ligands to the Mg^{2+}: O1 on the P1 phosphate and O5 on the P2 phosphate (see Figure 9). The Mg^{2+}−O bond distances are 1.9 and 1.8 Å, respectively. In addition, the Mg^{2+} ion is also coordinated to the Oγ1 of Thr 186 (1.9 Å) and Oγ of Ser 237 (1.8 Å) and to two solvent molecules (bond distances 1.9 and 2.0 Å). The geometry around the Mg^{2+} ion is almost regular octahedral, the two PP_i oxygen atoms and the two protein ligands lying in a perfect plane (the deviations from planarity range from 0.006 to 0.02 Å), with the Mg^{2+} ion lying directly in this plane (deviation ≈ 0.008 Å).

Comparison with MgADP•BeF_x•S1Dc. The polypeptide chain of $MgPP_i$•S1Dc closely resembles that of MgADP•BeF_x•S1Dc, which is not surprising considering the closely isomorphous nature of the crystals. The overall rms difference in main-chain atom positions between $MgPP_i$•S1Dc and MgADP•BeF_x•S1Dc, for all 743 amino acids, is 0.31 Å. As expected, there is a strong correlation between areas with highest deviations in atomic positions and those regions mentioned earlier as having large average main-chain temperature factors and/or low correlations between observed and calculated structure factors. These regions are primarily

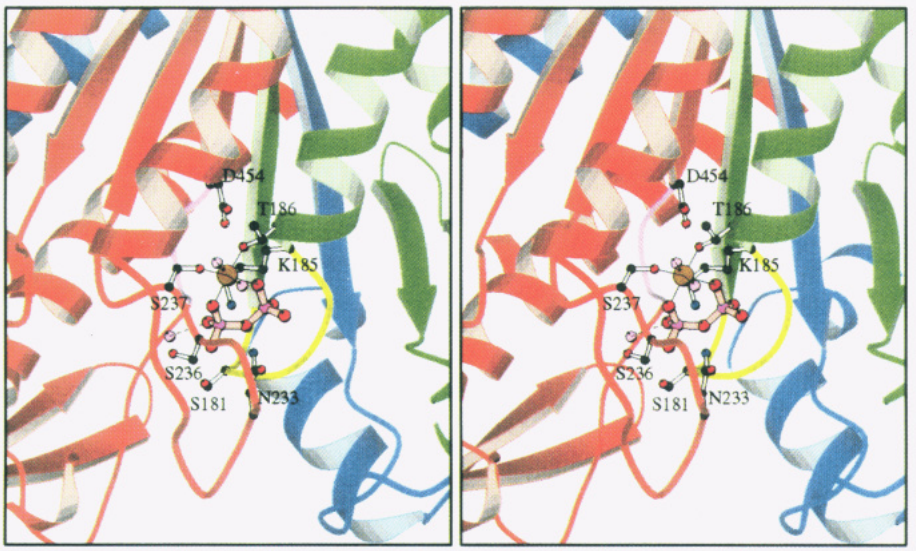

FIGURE 8: Stereo overview of the phosphate binding pocket, showing the location of the $MgPP_i$. The color coding of the domains is consistent with that previously used for the chicken S1 structure (Rayment et al., 1993b); the NH_2-terminal segment of the myosin heavy chain is shown in green, the central segment in red, and the COOH-terminal segment in blue. The central seven-stranded β-sheet can be clearly seen. The phosphate binding loop is shown in yellow and the D-X-X-G motif linking the top part of the central domain with the lower part is shown in pink. The locations of some key residues referred to in the paper are indicated. Both this figure and Figure 9 were produced with the program MOLSCRIPT (Kraulis, 1991).

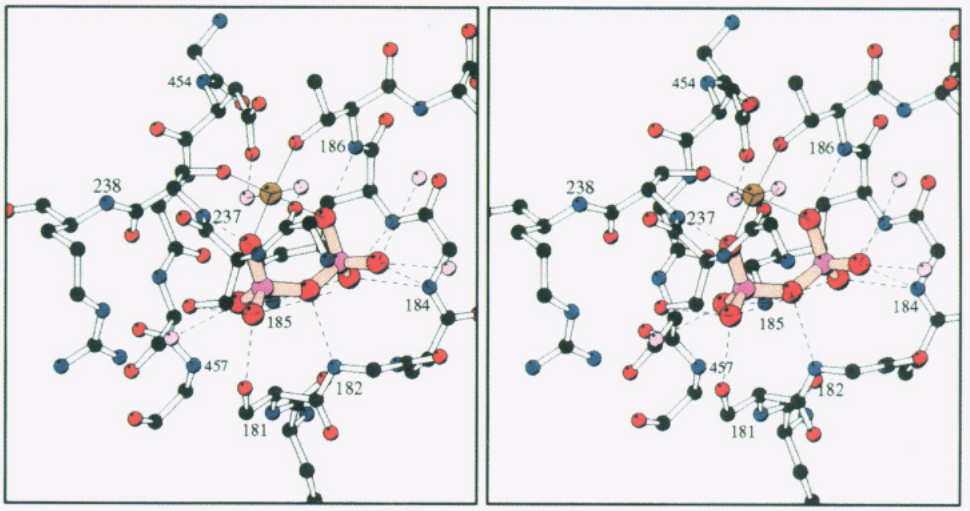

FIGURE 9: Detailed stereoview of the phosphate binding pocket and the $MgPP_i$ ion. The P-loop residues (Ser 181−Glu 187) are shown encompassing the pyrophosphate ion (pink bonds) to the left. The magnesium ion is indicated in orange, while solvent molecules are given in pink. All hydrogen-bonding interactions with the pyrophosphate, with the exception of those with the side chain of Asn 233, are given by dashed lines.

located at the surface of the molecule and appear quite flexible.

Superposition of the two molecules based only on the eight residues constituting the P-loop gives an rms deviation of only 0.35 Å (for all atoms in residues 179−187). The difference in the Mg^{2+} positions following this superposition is small (0.3 Å). Similarly, the β-phosphorus and the P1 phosphorus of the PP_i occupy essentially the same position (0.25 Å), and the oxygen atoms bonded to P1 of the PP_i are in identical positions to their counterparts on the β-phosphorus of the ADP. The P2 phosphorus almost exactly overlays the position occupied by the beryllium in MgADP·BeF_x·S1Dc; the rms difference is 0.1 Å. In addition, all of the other residues which make up the active site and the adenine binding site are in conserved positions, including eight water molecules (the average difference in positions for all atoms is 0.5 Å).

DISCUSSION

Pyrophosphate has been used extensively, along with AMPPNP and ATPγS, as a nonhydrolyzable analog of ATP to study the contractile cycle both in solution and in muscle fibers (Schoenberg, 1993). In fibers, the PP_i−myosin complex appears similar to the ATP−myosin complex, in that they both completely abolish the tension of muscle in the rigor state and weaken the binding of myosin to actin by increasing the dissociation rate constant (Schoenberg, 1991), even though this latter effect is significantly smaller for the $MgPP_i$ complex. It is expected that the conformational changes in myosin induced by both ATP and $MgPP_i$, which are responsible for the reduction in the binding affinity of myosin for actin, should be similar. The resulting conformation should represent a weakly binding state of myosin for actin.

The structure of the magnesium pyrophosphate complex of the truncated head of *Dictyostelium* myosin shows that pyrophosphate results in a conformation that is very similar to that observed in MgADP•BeF_x•S1Dc. Analysis of the active site indicates that the pyrophosphate molecule occupies the β- and γ-phosphate sites; the two phosphorus atoms are in the same positions as the β-phosphate and the BeF_x moiety of the beryllium fluoride-trapped ADP. The surrounding active site residues are almost perfectly superimposable in the two structures, and the hydrogen-bonding interactions that the PP_i makes with the protein are essentially identical. The similarity between the $MgPP_i$ and MgADP•BeF_x complex with S1Dc suggests that the conformational change that occurs when ATP binds to actomyosin and that reduces the affinity of myosin for actin is caused by the binding of the γ- and β-phosphate groups of the nucleotide. This then implies that the role of the remainder of the substrate is to increase the binding affinity of ATP for myosin and thus to drive the equilibrium toward dissociation of myosin from actin. These structures also suggest that the conformation observed here is representative of the weakly binding state of myosin for actin.

The structure of $MgPP_i$•S1Dc provides additional evidence that the MgADP•BeF_x•S1Dc complex is an accurate mimic of the prehydrolysis ATP-bound state of myosin since the phosphate groups of $MgPP_i$ bind in a very similar way to the beryllium fluoride moiety and the β-phosphate. The coordination observed here is very similar to that seen in the three-dimensional structures of the G-proteins, elongation factor Tu, and *ras*. In all of these proteins, the β- and γ-phosphate moieties of the nucleotides (either GTPγS or GMPPNP) all occupy identical positions, with respect to the structurally conserved phosphate binding loop, and interact with a divalent metal ion a conserved manner (unpublished data). In addition, several recent structural studies in this laboratory have shown that nonhydrolyzable ATP analogs including ATPγS, GMPPNP, and AMPPNP bind in an identical position to the MgADP•BeF_x complex and that the β- and γ-phosphate groups of these molecules overlay almost exactly the two phosphate groups of the pyrophosphate in $MgPP_i$•S1Dc (Smith, Fisher, and Rayment, unpublished data).

It is well established that myosin does not hydrolyze $MgPP_i$. As noted above, the S1Dc molecule adopts what is presumably the prehydrolysis (ATP-bound) state where the pyrophosphate molecule is located in a position similar to that of the β- and γ-phosphate groups of ATP. Furthermore, the interactions between PP_i and the protein are similar to those observed in MgADP•BeF_x. This raises the question of why $MgPP_i$ is not hydrolyzed by myosin? It has been suggested that the primary determinant in phosphate bond cleavage is the nature of the leaving group (Westheimer, 1987). Thus replacement of ADP by phosphate might account for the inability of myosin to hydrolyze PP_i due to the presence of an additional negative charge on the β-phosphate which is expected to yield a poorer leaving group than ADP. Alternatively, the inability to hydrolyze $MgPP_i$ might be due to the subtle differences in the water structure around the pyrophosphate moiety. These might prevent the protein from adopting the conformation observed in the MgADP•AlF_4 complex that has been predicted to be necessary for hydrolysis (Fisher et al., 1995).

In the original structural hypothesis for the contractile cycle it was proposed that when ATP binds to the actomyosin complex, it causes the narrow cleft that divides the central 50 kDa segment of motor domain of the myosin head to open, and this serves to disrupt the actin binding site and reduce the affinity of myosin for actin (Rayment et al., 1993a). Thereafter, it was envisaged that the nucleotide binding pocket closed around ATP and reconfigured the active site for hydrolysis. The three-dimensional structures of the motor domain from *D. discoideum* complexed with MgADP•BeF_x and $MgPP_i$ when compared to that of MgADP•AlF_4•S1Dc confirm that the narrow cleft that separates the upper and lower domains of the 50 kDa region plays a central role in the function of myosin. However, contrary to initial expectations the nucleotide binding pocket does not change significantly between these complexes (Fisher et al., 1995). These structures predict that the conformational change in myosin that is ultimately responsible for movement is associated with the COOH-terminal fragment of the myosin heavy chain that forms the interface with the essential light chains and contains the reactive sulfhydryl groups in skeletal muscle.

ACKNOWLEDGMENT

We thank Ralph Yount (Washington State University) for providing the ATP affinity column, Robert Smith for preparing the protein used in this investigation, and H. M. Holden, G. H. Reed, and W. W. Cleland (University of Wisconsin) for helpful discussions. We thank Siemens (Madison) for the loan a Hi-STAR double detector system used in this study.

REFERENCES

Abrahams, J. P., Leslie, A. G. W., Lutter, R., & Walker, J. E. (1994) *Nature 370*, 621−628.
Bagshaw, C. R., & Trentham, D. R. (1974) *Biochem. J. 141*, 331−349.
Balint, M., Sreter, F. A., Wolf, I., Nagy, B., & Gergley, J. (1975) *J. Biol. Chem. 250*, 6168−6177.
Bourne, H. R., Sanders, D. A., & McCormick, F. (1991) *Nature 349*, 117−127.
CCP4 (1994) *Acta Crystallogr. D50*, 760−763.
Coleman, D. E., Berghuis, A. M., Lee, E., Linder, M. E., Gilman, A. G., & Sprang, S. R. (1994) *Science 265*, 1405−1412.
Diederichs, K., & Schulz, G. E. (1990) *Biochemistry 29*, 8138−8144.
Eisenberg, E., & Greene, L. E. (1980) *Annu. Rev. Physiol. 42*, 293−309.
Fisher, A. J., Smith, C. A., Thoden, J., Smith, R., Sutoh, K., Holden, H. M., & Rayment, I. (1995) *Biochemistry 34*, 8960−8972.
Geeves, M. A., Goody, R. S., & Gutfreund, H. (1984) *J. Muscle Res. Cell Motil. 5*, 351−361.
Goldman, Y. E. (1987) *Annu. Rev. Physiol. 49*, 637−654.
Greene, L. E., & Eisenberg, E. (1980) *J. Biol. Chem. 255*, 543−548.
Holmes, K. C., Popp, D., Gebhard, W., & Kabsch, W. (1990) *Nature 347*, 44−49.
Itakura, S., Yamakawa, H., Toyoshima, Y. Y., Ishijima, A., Kojima, T., Harada, Y., Yamnagida, T., Wakabayashi, T., & Sutoh, K. (1993) *Biochem. Biophys. Res. Commun. 196*, 1504−1510.
Jones, T. A. (1985) in *Methods in Enzymology* (Wycoff, H. W., Hirs, C. H. W., & Timasheff, S. N., Eds.) pp 157−171, Academic Press Inc., New York.
Kabsch, W. (1988a) *J. Appl. Crystallogr. 21*, 67−71.
Kabsch, W. (1988b) *J. Appl. Crystallogr. 21*, 916−924.
Kabsch, W., Mannherz, H. G., Suck, D., Pai, E. F., & Holmes, K. C. (1990) *Nature 347*, 37−44.
Kjeldgaard, M., Nissen, P., Thirup, S., & Nyborg, J. (1993) *Structure 1*, 35−50.
Kraulis, P. J. (1991) *J. Appl. Crystallogr. 24*, 946−950.

Luzzati, V. (1952) *Acta Crystallogr. 5*, 802−810.
Lymn, R. W., & Taylor, E. W. (1971) *Biochemistry 10*, 4617−4624.
Matthews, B. W. (1968) *J. Mol. Biol. 33*, 491−497.
Mornet, D., Pantel, P., Audemard, E., & Kassab, R. (1979) *Biochem. Biophys. Res. Commun. 89*, 925−932.
Muller, C. W., & Schulz, G. E. (1992) *J. Mol. Biol. 224*, 159−177.
Noel, J. P., Hamm, H. E., & Sigler, P. B. (1993) *Nature 366*, 654−663.
Pai, E. F., Krengel, U., Petsko, G. A., Goody, R. S., Kabsch, W., & Wittinghofer, A. (1990) *EMBO J. 9*, 2351−2359.
Ramakrishnan, C., & Ramachandran, G. N. (1965) *Biophys. J. 5*, 909−933.
Rayment, I., Holden, H. M., Whittaker, M., Yohn, C. B., Lorenz, M., Holmes, K. C., & Milligan, R. A. (1993a) *Science 261*, 58−65.
Rayment, I., Rypniewski, W. R., Schmidt-Bäse, K., Smith, R., Tomchick, D. R., Benning, M. M., Winkelmann, D. A., Wesenberg, G., & Holden, H. M. (1993b) *Science 261*, 50−58.
Read, R. J. (1986) *Acta Crystallogr. A42*, 140−149.
Ritchie, M. D., Geeves, M. A., Woodward, S. K. A., & Manstein, D. J. (1993) *Proc. Natl. Acad. Sci. U.S.A. 90*, 8619−8623.
Schoenberg, M. (1991) *Biophys. J. 60*, 690−696.
Schoenberg, M. (1993) *Adv. Biophys. 26*, 55−73.
Sondek, J., Lambright, D. G., Noel, J. P., Hamm, H. E., & Sigler, P. B. (1994) *Nature 372*, 276−279.
Stein, L. A., Schwarz, R. P. J., Chock, P. B., & Eisenberg, E. (1979) *Biochemistry 18*, 3895−3909.
Story, R. M., & Steitz, T. A. (1992) *Nature 355*, 374−376.
Tronrud, D. E., Ten Eyck, L. F., & Matthews, B. W. (1987) *Acta Crystallogr. A43*, 489−501.
Trybus, K. M., & Taylor, E. W. (1982) *Biochemistry 21*, 1284−1294.
Westheimer, F. H. (1987) *Science 235*.
Wilson, A. J. C. (1942) *Nature 150*, 152.
Yount, R. G., Ojala, D., & Babcock, D. (1971) *Biochemistry 10*, 2490−2495.

BI9507903